



Threonine stabilizer-controlled well-dispersed small palladium nanoparticles on modified magnetic nanocatalyst for Heck cross-coupling process in water

Iraj Sarvi | Mostafa Gholizadeh | Mohammad Izadyar

Department of Chemistry, Faculty of Science, Ferdowsi University of Mashhad, Mashhad 91775-1436, Iran

Correspondence

Mostafa Gholizadeh, Department of Chemistry, Faculty of Science, Ferdowsi University of Mashhad, Mashhad 91775-1436, Iran.

Email: m_gholizadeh@um.ac.ir

Funding information

Ferdowsi University of Mashhad, Grant/Award Number: 3/41258

We report the synthesis of magnetically separable Fe₃O₄@Silica-Threonine-Pd⁰ magnetic nanoparticles with a core-shell structure. After synthesis of Fe₃O₄@Silica, threonine as an efficient stabilizer/ligand was bonded to the surface of Fe₃O₄@Silica. Then, palladium nanoparticles were generated on the threonine-modified catalyst. The threonine stabilizer helps to generate palladium nanoparticles of small size (less than 4 nm) with high dispersity and uniformity. Magnetically separable Fe₃O₄@Silica-Threonine-Pd⁰ nanocatalyst was fully characterized using various techniques. This nanocatalyst efficiently catalysed the Heck cross-coupling reaction of a variety of substrates in water medium as a green, safe and inexpensive solvent at 80°C. The Fe₃O₄@Silica-Threonine-Pd⁰ catalyst was used for at least eight successful consecutive runs with palladium leaching of only 0.05%.

KEYWORDS

Heck cross-coupling reaction, magnetic catalyst, small palladium nanoparticles, threonine stabilizer

1 | INTRODUCTION

Environmentally friendly heterogeneous catalytic systems have strongly stimulated growth in modern chemical transformations.^[1–3] In this regard, safer, cleaner, simpler and greener approaches have been considered for developing sustainable and environmentally friendly methods. For this purpose, nanoparticles supported on modified organic–inorganic hybrid surfaces with high selectivity and recyclability have been investigated.^[4,5] The palladium-catalysed carbon–carbon bond forming reaction is considered as a powerful synthetic tool and a major area in catalysis, organic transformations and pharmaceutical, agrochemical and fine chemical industries.^[6] Among them, Heck–Mizoroki cross-coupling is one of the most beneficial reactions for carbon–carbon bond formation due to its high efficiency and atom economy.^[7] During the last few decades, various homogeneous, heterogeneous and organometallic systems with special

ligands have been developed for the Heck cross-coupling reaction.^[8–10] Most of them suffer from drawbacks such as tedious multistep synthesis and work-up, air- and moisture-sensitive ligands, expensive, unstable and toxic ligands such as phosphine, and use of various additives and harmful solvents.^[11,12] Also, a diverse array of organic and inorganic supports, such as polymers, carbon, clay, ordered silicates and zeolites, have been used as hosts for palladium nanoparticles in cross-coupling reactions.^[13–17] Magnetic nanoparticles as a readily available and low-cost material with high surface area, high catalyst loading capacity and high stability have also been used.^[18] They can be modified, coated and functionalized with various ligands/stabilizers and hybrid precursors. Based on the literature, particle size, crystal structure and nature of the ligand are crucial in the activity of nanocatalysts.^[19–21] Aggregation/oxidation of metal nanoparticles, which causes decreased catalytic performance, can be avoided by a well-chosen

ligand/stabilizer. The particle size, shape, magnetic features and chemical stability of the hybrid materials can be controlled with such stabilizers. A stabilizer prevents the agglomeration of metal species.^[22]

As a part of our ongoing researches on novel heterogeneous catalysis and designing and developing environmentally benign green methods in catalysis,^[23–26] our aim has been to investigate efficient magnetically recoverable palladium-based nanocatalysts with high activity for the Heck cross-coupling reaction under mild conditions with minimum by-products and high yields. In the work reported herein, we used silica-coated magnetic nanoparticles ($\text{Fe}_3\text{O}_4@\text{SiO}_2$) as a recoverable and reusable support. The surface of $\text{Fe}_3\text{O}_4@\text{SiO}_2$ was modified with the amino acid threonine with $-\text{NH}_2$ and $-\text{OH}$ groups serving as a suitable stabilizer for immobilization of small palladium nanoparticles without any time-consuming steps for the synthesis of the ligand. The use of less toxic and inexpensive palladium-based threonine-functionalized $\text{Fe}_3\text{O}_4@\text{SiO}_2$ catalysts has not been reported to date for the Heck reaction. A schematic pathway for preparation of Pd^0 immobilized on threonine-modified $\text{Fe}_3\text{O}_4@\text{SiO}_2$ magnetic nanoparticles (FST-Pd⁰ MNPs) is illustrated in Scheme 1.

2 | EXPERIMENTAL

2.1 | Materials and apparatus

Palladium chloride (PdCl_2), L-threonine ($\text{C}_4\text{H}_9\text{NO}_3$), iron(III) chloride hexahydrate ($\text{FeCl}_3 \cdot 6\text{H}_2\text{O}$), sodium acetate (NaOAc), trisodium citrate (Na_3Cit), tetraethyl orthosilicate ($\text{SiC}_8\text{H}_{20}\text{O}_4$) and other compounds were obtained from Sigma-Aldrich and Merck of analytical grade and used without further purification. For morphology and size study of the as-prepared samples, transmission electron microscopy (TEM) and scanning electron microscopy (SEM) experiments were conducted with a Leo 912AB microscope (Germany) operated at 120 kV and a Leo 1450VP microscope (Germany),

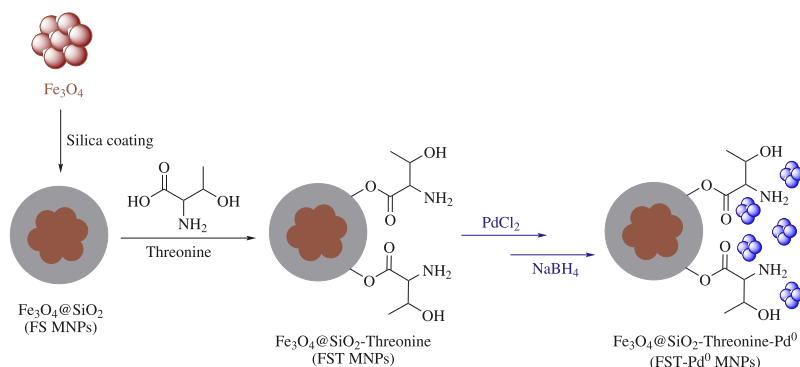
respectively. Wide-angle X-ray diffraction (XRD) patterns were recorded using a Bruker D4 X-ray diffractometer (Germany) with Ni-filtered Cu KR radiation (40 kV, 40 mA). The percentage weight loss of shell and arginine was studied using thermogravimetric analysis (TGA; Mettler Toledo LF, Switzerland). Fourier transform infrared (FT-IR) spectra were collected with a Nicolet Fourier spectrophotometer (USA), using KBr pellets. To investigate the magnetic behaviour of the catalyst, vibrating sample magnetometry (VSM; 7400 Lake Shore, USA) was used. ¹H NMR and ¹³C NMR spectra were measured (CDCl_3) with a Bruker DRX-300 AVANCE spectrometer at 300 and 75 MHz, respectively. The contents of palladium on the prepared solid catalysts and palladium leaching were measured using inductively coupled plasma optical emission spectrometry (ICP-OES) with an Avio 200 ICP instrument.

2.2 | Synthesis of Fe_3O_4 magnetic nanoparticles (MNPs)

Based on a previously reported procedure, Fe_3O_4 MNPs were prepared hydrothermally.^[27] At first, $\text{FeCl}_3 \cdot 6\text{H}_2\text{O}$ (3 mmol, 0.81 g), NaOAc (24.4 mmol, 2.0 g) and Na_3Cit (2.9 mmol, 0.75 g) were dissolved in 40 ml of ethylene glycol and stirred vigorously for 1 h. The obtained yellow solution was transferred into a Teflon-lined stainless steel autoclave (50 ml capacity) and heated at 200°C for 12 h. After completion of the reaction, the autoclave was cooled to room temperature. The obtained black Fe_3O_4 MNPs were collected with a magnet and washed with water and ethanol. The final precipitate was then dried under vacuum at 50°C for 4 h.^[27]

2.3 | Synthesis of $\text{Fe}_3\text{O}_4@\text{Silica@Threonine}$ magnetic nanoparticles (FST MNPs)

Fe_3O_4 powder (0.1 g) was dispersed in HNO_3 (5 ml, 0.1 M) solution with ultrasonication for 20 min, and then



SCHEME 1 Schematic representation of catalyst preparation (FST-Pd⁰ MNPs)

washed with deionized water. The post-treated Fe₃O₄ nanoparticles were dispersed in water (6 ml, 0.05 g) and then added to 500 ml of absolute ethanol and 130 ml of deionized water. Ammonia solution (28 wt%, 10 ml) was added to this mixture under sonication in 30 min. Then, tetraethyl orthosilicate (8.0 ml, 7.46 g) was added dropwise under stirring for 12 h. After separation, Fe₃O₄@SiO₂ was washed with water and ethanol three times.^[23] Finally, 0.1 g of Fe₃O₄@SiO₂ and threonine (16.8 mmol, 2 g) were dispersed in 40 ml of a mixture of EtOH and water (1:1) and then sealed in a 50 ml autoclave at 150°C for 2 h. The FST MNPs were collected with a magnet and washed several times with water and ethanol and dried at 50°C in an oven.

2.4 | Synthesis of Fe₃O₄@SiO₂@Threonine-Pd⁰ (FST-Pd⁰) nanoparticles

FST MNPs (0.2 g) were dispersed in 15 ml of distilled water for 10 min. An aqueous solution of PdCl₂ (5 ml, 0.1 M) was added to the mixture and stirred for 12 h. The acquired FST-Pd^{II} MNPs were separated from the solution and washed with hot water and ethanol five times. Finally, FST-Pd^{II} MNPs were treated with an aqueous solution of NaBH₄ (10 ml, 0.05 M) for 6 h in an ice bath. The FST-Pd⁰ thus produced was then collected with a magnet and washed four times with water and ethanol.

2.5 | Typical procedure for Heck cross-coupling reaction

To a mixture of Et₃N (2 mmol, 0.2 g), methyl acrylate (1.2 mmol, 0.1 g) and bromobenzene (1 mmol, 0.16 g) in water (1.5 ml, 1.5 g), 0.25 mol% of FST-Pd⁰ MNPs was added and heated at 80°C in an oil bath. After completion of the reaction (monitored by TLC) the nanocatalyst was separated using a magnet and washed with ethyl acetate three times. The reaction mixture was extracted with ethyl acetate (3 × 5 ml) and the organic layer was dried over anhydrous MgSO₄. Finally, solvent was evaporated and the crude product purified by column chromatography (*n*-hexane–ethyl acetate, 10:2).

2.5.1 | Methyl cinnamate (3a)

¹H NMR (CDCl₃, 300 MHz, δ, ppm): 3.83 (s, 3H), 6.47 (d, 1H, *J* = 12 Hz), 7.40 (m, 3H), 7.54 (m, 2H), 7.73 (d, 1H, *J* = 12 Hz). ¹³C NMR (CDCl₃, 75 MHz, δ, ppm): 52.54, 118.65, 128.94, 129.75, 131.16, 135.23, 145.72, 168.26.

2.5.2 | Ethyl cinnamate (3b)

¹H NMR (CDCl₃, 300 MHz, δ, ppm): 1.37 (t, 3H, *J* = 6 Hz), 4.30 (q, 2H, *J* = 6 Hz), 6.47 (d, 1H, *J* = 12 Hz), 7.40–7.43 (m, 3H), 7.54–7.57 (m, 2H), 7.72 (d, 1H, *J* = 12 Hz). ¹³C NMR (CDCl₃, 75 MHz, δ, ppm): 15.01, 30.56, 61.37, 119.13, 128.91, 129.73, 131.07, 135.32, 145.45, 167.88.

2.5.3 | Butyl cinnamate (3c)

¹H NMR (CDCl₃, 300 MHz, δ, ppm): 1.00 (t, 3H, *J* = 6 Hz), 1.48 (sex, 2H, *J* = 6, 3 Hz), 1.74 (pen, 2H, *J* = 9, 3 Hz), 4.25 (t, 2H, *J* = 6 Hz), 6.47 (d, 1H, *J* = 12 Hz), 7.39–7.42 (m, 3H), 7.54–7.56 (m, 2H), 7.72 (d, 1H, *J* = 12 Hz). ¹³C NMR (CDCl₃, 75 MHz, δ, ppm): 14.62, 20.07, 31.64, 65.28, 119.14, 128.91, 129.72, 131.06, 135.33, 145.41, 167.95.

2.5.4 | Methyl-3-(*p*-tolyl) acrylate (3d)

¹H NMR (CDCl₃, 300 MHz, δ, ppm): 2.40 (s, 3H), 3.83 (s, 3H), 6.43 (d, 1H, *J* = 12 Hz), 7.22 (d, 2H, *J* = 6 Hz), 7.45 (d, 2H, *J* = 6 Hz), 7.70 (d, 1H, *J* = 12 Hz). ¹³C NMR (CDCl₃, 75 MHz, δ, ppm): 22.32, 52.49, 117.54, 128.93, 130.48, 132.50, 141.58, 145.74, 168.50.

2.5.5 | Ethyl-3-(*p*-tolyl) acrylate (3e)

¹H NMR (CDCl₃, 300 MHz, δ, ppm): 1.36 (t, 3H, *J* = 6 Hz), 2.39 (s, 3H), 4.29 (q, 2H, *J* = 6 Hz), 6.42 (d, 1H, *J* = 12 Hz), 7.20 (d, 2H, *J* = 6 Hz), 7.44 (d, 2H, *J* = 6 Hz), 7.69 (d, 1H, *J* = 12 Hz). ¹³C NMR (CDCl₃, 75 MHz, δ, ppm): 15.20, 22.29, 61.24, 118.01, 128.90, 130.46, 132.59, 141.45, 145.44, 168.02.

2.5.6 | Butyl-3-(*p*-tolyl) acrylate (3f)

¹H NMR (CDCl₃, 300 MHz, δ, ppm): 1.00 (t, 3H, *J* = 6 Hz), 1.48 (sex, 2H, *J* = 6, 3 Hz), 1.73 (pen, 2H, *J* = 9, 6 Hz), 2.39 (s, 3H), 4.24 (t, 2H, *J* = 6 Hz), 6.43 (d, 1H, *J* = 12 Hz), 7.21 (d, 2H, *J* = 6 Hz), 7.45 (d, 2H, *J* = 6 Hz), 7.69 (d, 1H, *J* = 12 Hz). ¹³C NMR (CDCl₃, 75 MHz, δ, ppm): 14.62, 20.08, 22.29, 31.67, 65.17, 118.03, 128.90, 130.45, 132.60, 141.44, 145.40, 168.13.

2.5.7 | Ethyl-3-(4-ethylphenyl) acrylate (3g)

^1H NMR (CDCl_3 , 300 MHz, δ , ppm): 1.26 (t, 3H, $J = 12$ Hz), 1.36 (t, 3H, $J = 12$ Hz), 2.68 (q, 2H, $J = 6$ Hz), 4.28 (q, 2H, $J = 6$ Hz), 6.43 (d, 1H, $J = 12$ Hz), 7.23 (d, 2H, $J = 6$ Hz), 7.46 (d, 2H, $J = 6$ Hz), 7.70 (d, 1H, $J = 12$ Hz). ^{13}C NMR (CDCl_3 , 75 MHz, δ , ppm): 15.19, 16.17, 29.64, 61.23, 118.05, 129.00, 129.26, 132.83, 145.46, 147.74, 168.02.

2.5.8 | Butyl-3-(4-ethylphenyl) acrylate (3h)

^1H NMR (CDCl_3 , 300 MHz, δ , ppm): 1.00 (t, 3H, $J = 6$ Hz), 1.27 (t, 3H, $J = 6$ Hz), 1.47 (sex, 2H, $J = 6$, 3 Hz), 1.73 (pen, 2H, $J = 9$, 3 Hz), 2.69 (q, 2H, $J = 6$ Hz), 4.24 (t, 2H, $J = 6$ Hz), 6.43 (d, 1H, $J = 12$ Hz), 7.24 (d, 2H, $J = 6$ Hz), 7.48 (d, 2H, $J = 6$ Hz), 7.70 (d, 1H, $J = 12$ Hz). ^{13}C NMR (CDCl_3 , 75 MHz, δ , ppm): 14.62, 16.18, 20.07, 29.65, 31.66, 65.19, 118.08, 129.00, 129.27, 132.84, 145.43, 147.76, 168.16.

2.5.9 | Methyl-3-(4-methoxyphenyl) acrylate (3i)

^1H NMR (CDCl_3 , 300 MHz, δ , ppm): 2.42 (s, 3H), 3.85 (s, 3H), 6.41 (d, 1H, $J = 12$ Hz), 7.19 (d, 2H, $J = 6$ Hz), 7.42 (d, 2H, $J = 6$ Hz), 7.68 (d, 1H, $J = 12$ Hz). ^{13}C NMR (CDCl_3 , 75 MHz, δ , ppm): 22.30, 52.38, 117.68, 128.91, 130.49, 132.52, 141.68, 145.69, 168.49.

2.5.10 | Ethyl-3-(4-methoxyphenyl) acrylate (3j)

^1H NMR (CDCl_3 , 300 MHz, δ , ppm): 1.34 (t, 3H, $J = 6$ Hz), 3.83 (s, 3H), 4.26 (q, 2H, $J = 9$ Hz), 6.32 (d, 1H, $J = 12$ Hz), 6.90 (d, 2H, $J = 3$ Hz), 7.41 (d, 2H, $J = 3$ Hz), 7.66 (d, 2H, $J = 12$ Hz). ^{13}C NMR (CDCl_3 , 75 MHz, δ , ppm): 15.20, 56.16, 61.14, 115.14, 116.56, 128.01, 130.52, 145.08, 162.18, 168.15.

2.5.11 | Butyl-3-(4-methoxyphenyl) acrylate (3k)

^1H NMR (CDCl_3 , 300 MHz, δ , ppm): 0.99 (t, 3H, $J = 6$ Hz), 1.46 (sex, 2H, $J = 6$, 3 Hz), 1.70 (pen, 2H, $J = 9$, 3 Hz), 3.85 (s, 3H), 4.23 (t, 2H, $J = 12$ Hz), 6.34 (d, 1H, $J = 12$ Hz), 6.93 (d, 2H, $J = 6$ Hz), 7.50 (d, 2H, $J = 6$ Hz), 7.66 (d, 1H, $J = 12$ Hz). ^{13}C NMR (CDCl_3 ,

75 MHz, δ , ppm): 14.62, 20.07, 31.67, 56.20, 65.11, 115.15, 116.61, 128.06, 130.54, 145.06, 162.17, 168.30.

2.5.12 | Methyl-3-(4-formylphenyl) acrylate (3l)

^1H NMR (CDCl_3 , 300 MHz, δ , ppm): 3.86 (s, 3H), 6.58 (d, 1H, $J = 12$ Hz), 7.71 (d, 2H, $J = 6$ Hz), 7.75 (d, 1H, $J = 12$ Hz), 7.93 (d, 2H, $J = 6$ Hz), 10.02 (s, 1H). ^{13}C NMR (CDCl_3 , 75 MHz, δ , ppm): 52.85, 121.83, 129.39, 131.04, 138.03, 140.89, 144.00, 167.68, 192.33.

2.5.13 | Ethyl-3-(4-formylphenyl) acrylate (3m)

^1H NMR (CDCl_3 , 300 MHz, δ , ppm): 1.34 (t, 3H, $J = 6$ Hz), 4.27 (q, 2H, $J = 6$ Hz), 6.54 (d, 1H, $J = 12$ Hz), 6.66 (d, 2H, $J = 6$ Hz), 7.69 (d, 1H, $J = 12$ Hz), 7.88 (d, 2H, $J = 6$ Hz), 10.01 (s, 1H). ^{13}C NMR (CDCl_3 , 75 MHz, δ , ppm): 15.11, 61.65, 122.29, 129.32, 130.98, 137.96, 140.94, 143.63, 167.15, 192.27.

2.5.14 | Butyl-3-(4-formylphenyl) acrylate (3n)

^1H NMR (CDCl_3 , 300 MHz, δ , ppm): 0.98 (t, 3H, $J = 6$ Hz), 1.45 (sex, 2H, $J = 12$, 6 Hz), 1.72 (pen, 2H, $J = 9$, 6 Hz), 4.24 (t, 2H, $J = 6$ Hz), 6.57 (d, 1H, $J = 12$ Hz), 7.69 (d, 2H, $J = 6$ Hz), 7.72 (d, 1H, $J = 12$ Hz), 7.91 (d, 2H, $J = 6$ Hz), 10.04 (s, 1H). ^{13}C NMR (CDCl_3 , 75 MHz, δ , ppm): 14.59, 20.02, 31.55, 65.62, 122.32, 129.35, 131.02, 137.95, 140.98, 143.66, 167.33, 192.35.

2.5.15 | Methyl-3-(4-cyanophenyl) acrylate (3o)

^1H NMR (CDCl_3 , 300 MHz, δ , ppm): 3.84 (s, 3H), 6.54 (d, 1H, $J = 12$ Hz), 7.62–7.71 (m, 5H). ^{13}C NMR (CDCl_3 , 75 MHz, δ , ppm): 52.88, 114.27, 119.20, 122.23, 129.26, 133.51, 139.49, 143.27, 167.43.

2.5.16 | Ethyl-3-(4-cyanophenyl) acrylate (3p)

^1H NMR (CDCl_3 , 300 MHz, δ , ppm): 1.37 (t, 3H, $J = 6$ Hz), 4.31 (q, 2H, $J = 6$ Hz), 6.54 (d, 1H, $J = 12$ Hz), 7.62–7.71 (m, 5H). ^{13}C NMR (CDCl_3 , 75 MHz, δ , ppm): 15.12, 61.80, 114.20, 119.23, 122.73, 129.23, 133.50, 139.60, 142.98, 167.00.

2.5.17 | Butyl-3-(4-cyanophenyl) acrylate (3q)

^1H NMR (CDCl_3 , 300 MHz, δ , ppm): 0.96 (t, 3H, $J = 6$ Hz), 1.43 (sex, 2H, $J = 9, 6$ Hz), 1.69 (pen, 2H, $J = 9, 6$ Hz), 4.22 (t, 2H, $J = 6$ Hz), 6.52 (d, 1H, $J = 12$ Hz), 7.60–7.69 (m, 5H). ^{13}C NMR (CDCl_3 , 75 MHz, δ , ppm): 14.56, 19.99, 31.52, 65.64, 114.14, 119.20, 122.71, 129.23, 133.46, 139.58, 142.92, 167.04.

3 | RESULTS AND DISCUSSION

In the first step, Fe_3O_4 MNPs were prepared via a hydrothermal process and then coated with a silica shell using the Stöber method^[23] to achieve the $\text{Fe}_3\text{O}_4@\text{SiO}_2$ MNPs as a support. In the next step, threonine as an efficient ligand/stabilizer was bonded on the surface of FS MNPs. Finally, PdCl_2 was added to threonine-modified FS MNPs. After chemical reduction of loaded Pd^{II} ions with NaBH_4 , small Pd^0 nanoparticles were generated and dispersed uniformly on the surface of the nanocatalyst. The chemical structure of the catalyst was studied with FT-IR spectroscopy (Figure 1). As shown in Figure 1a, the characteristic peak at 565 cm^{-1} was attributed to the stretching vibration of the Fe–O bond of Fe_3O_4 MNPs. After surface coating with silica shell, the intensity of the Fe–O stretching band was significantly decreased and a strong absorption peak at 1100 cm^{-1} and weak absorption peak at 950 cm^{-1} appeared in the FT-IR spectrum of FS MNPs for asymmetric vibration of the Si–O–Si bond and symmetric stretching of the Si–OH bond, respectively (Figure 1b in comparison with Figure 1a) which confirm that magnetic core was successfully coated with the silica shell. The FT-IR spectrum of threonine revealed characteristic peaks at 3155, 1678, 2928 and 1464 cm^{-1} , corresponding to NH_2 stretching, NH_2 out-of-plane bending, asymmetric stretching and asymmetric

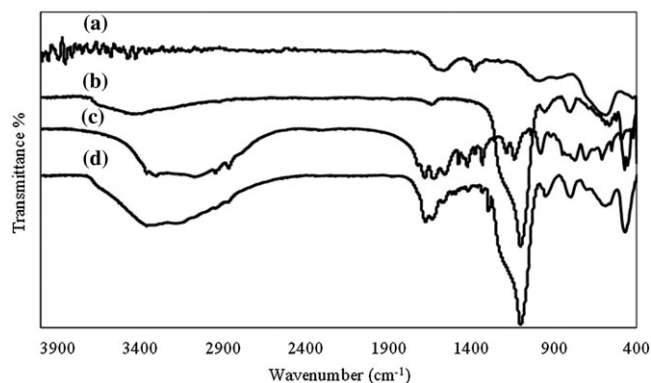


FIGURE 1 FT-IR spectra of (a) Fe_3O_4 MNPs, (b) FS MNPs, (c) threonine and (d) FST MNPs

bending of CH_2 and CH_3 groups, respectively (Figure 1c). Also, two bands at 1574 and 1535 cm^{-1} in Figure 1c can be attributed to the stretching vibration of CO and bending vibration of OH groups. In the FT-IR spectrum of serine-modified FS MNPs (Figure 1d), characteristic peaks of threonine, Fe–O stretching vibration of magnetic core and silica shell can be observed that confirm the functionalization of the FS MNPs with threonine ligands and the magnetic nature of the catalyst.^[28]

For thermal stability study of the nanocatalyst and calculation of the amount of organic moieties on the surface of the nanocatalyst, TGA was carried out in a static nitrogen atmosphere (Figure 2). The FST-Pd MNPs revealed different weight loss in the temperature range $30\text{--}800^\circ\text{C}$. Initial weight loss up to 150°C was probably due to the removal of surface hydroxyls and surface adsorbed water, while the weight loss at $200\text{--}600^\circ\text{C}$ was attributed mainly to the decomposition of organic groups from the catalyst surface. These results clearly corroborated that organic functional groups were incorporated on the surface of FST-Pd 0 MNPs.

The crystallographic structures of FS MNPs and FST-Pd 0 MNPs were investigated using the XRD technique as shown in Figure 3. Six diffraction peaks located at 30.35° (220), 35.44° (311), 43.31° (400), 53.14° (422), 56.87° (511) and 62.51° (440) in the XRD patterns of FS MNPs and FST-Pd 0 MNPs can be assigned to diffraction peaks of the Fe_3O_4 crystalline phase, according to JCPDS card no. 19-0629. Based on these results, the crystalline structure of the magnetic core remained unchanged after the chemical modification and reduction processes. No other diffraction peaks can be seen in Figure 3a, which confirms the purity of the Fe_3O_4 crystalline phase. Also, the Fe_3O_4 core exhibits a cluster-like nanostructure with an average crystalline size of 15 nm calculated using the Debye–Scherrer equation from the broadness of the (311) peak. As shown in Figure 3b, the intensities of Fe_3O_4 diffraction peaks were decreased due to the heavy atom effect of Pd nanoparticles. Three new diffraction

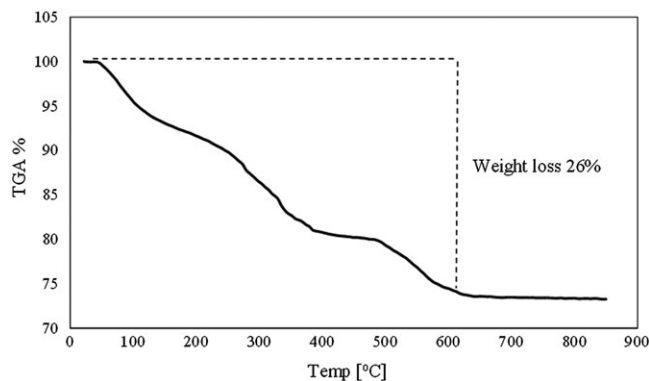


FIGURE 2 TGA curve of FST-Pd 0 MNPs

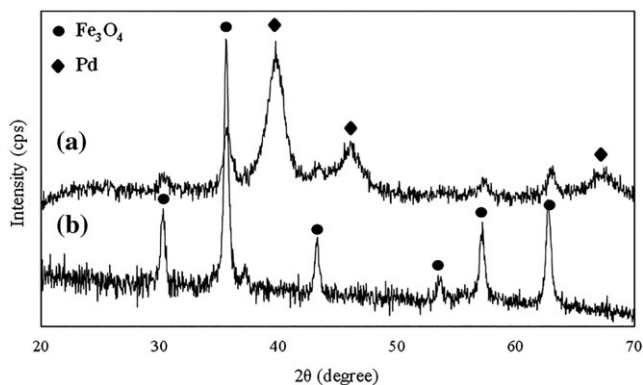


FIGURE 3 XRD patterns of (a) Fe_3O_4 MNPs and (b) FST- Pd^0 MNPs

peaks located at 39.79° (111), 46.10° (200) and 67.15° (220) were appeared in Figure 3a which were assigned to a face-centred cubic structure of Pd according to JCPDS card no. 46-1043. The average size of Pd nanoparticles was calculated as 2.5 nm using the broadness of the (111) peak.

The magnetic properties of Fe_3O_4 MNPs and FST- Pd^0 MNPs were investigated using VSM. As illustrated in Figure 4, both samples have a ferromagnetic nature. Saturation magnetization values of Fe_3O_4 MNPs and FST- Pd^0 MNPs were 59.50 and 38.75 emu g^{-1} , respectively. Due to the greater mass and size of the silica shell, organic ligand and metallic species, the saturation magnetization value of FST- Pd^0 MNPs (Figure 4b) was decreased in comparison with that of Fe_3O_4 MNPs (Figure 4a). The saturation magnetization of the nanocatalyst was high enough to provide easy and quick separation from a reaction mixture with an external magnet.

The size and morphology of the nanocatalyst were studied using SEM and TEM (Figure 5). Based on the TEM image of Fe_3O_4 MNPs in Figure 5a, magnetic nanoparticles are approximately spherical particles (Figure 5

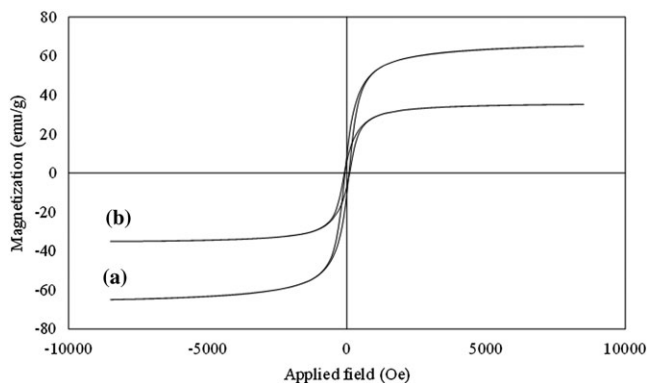


FIGURE 4 Magnetization hysteresis loops of (a) Fe_3O_4 MNPs and (b) FST- Pd^0 MNPs

a). After the silica coating process, the TEM image of FS MNPs (Figure 5b) showed that the magnetic core was well encapsulated by the silica shell and a clear boundary between the silica shell and magnetic core was observed in the core-shell morphology (Figure 5b). After Pd^{II} ions were loaded on the surface -- NH_2 and -- OH groups of FST MNPs and the reduction process, uniformly dispersed small Pd^0 nanoparticles on the siliceous shell of the catalyst were observed with particle sizes in the range 5–20 nm in the TEM image (Figure 5c). Based on this observation, Pd nanoparticle size and distribution have been controlled in the presence of the threonine stabilizer/ligand. The SEM image of FST- Pd^0 MNPs (Figure 5d) showed spherical morphology of the nanocatalyst. Also, aggregation of nanoparticles was observed due to the magnetic nature of the catalyst. The energy-dispersive X-ray analysis result (Figure 5e) indicated that the elemental composition of FST- Pd^0 MNPs is Fe (21.2%), O (45.8%), Si (31.5%) and Pd (1.5%), which can be attributed to the existence of Fe_3O_4 core, silica shell and dispersed Pd nanoparticles. The content of Pd nanoparticles in the sample was confirmed using ICP-OES. The amount of Pd nanoparticles loaded onto the FCA was 8.5 wt%.

After successful synthesis and characterization of the designed nanocatalyst, its efficiency was evaluated in C-C bond formation via the Heck cross-coupling reaction.

The catalytic activity of FST- Pd^0 MNPs was investigated in the Heck cross-coupling of bromobenzene (1 mmol) and methyl acrylate (1.2 mmol) as a model reaction. For this purpose, the effects of various parameters such as solvent, base, reaction temperature and catalyst amount were examined in the model reaction (Table 1).

The effect of various solvents on the model reaction was investigated as a first step (Table 1, entries 1–8). Polar and non-polar solvents such as dimethylformamide (DMF), dimethylsulfoxide (DMSO), tetrahydrofuran (THF), *n*-hexane, toluene, 1,4-dioxane, ethanol and water were examined in the presence of 1 mol% of catalyst, among which water can be used as a green, non-toxic and inexpensive solvent for the model reaction. In the following step, several common bases were examined in the model reaction. The results revealed that the presence of base has a crucial effect in the Heck cross-coupling reaction progress (Table 1, entries 8–12). Et_3N afforded higher yield and shorter reaction time than the other bases (Table 1, entry 12). Also, reaction temperature was evaluated in the model reaction. The best result was achieved when the model reaction was carried out at 80°C (Table 1, entries 13–15). The amount of catalyst was also optimized. Higher yield of the desired product in shorter

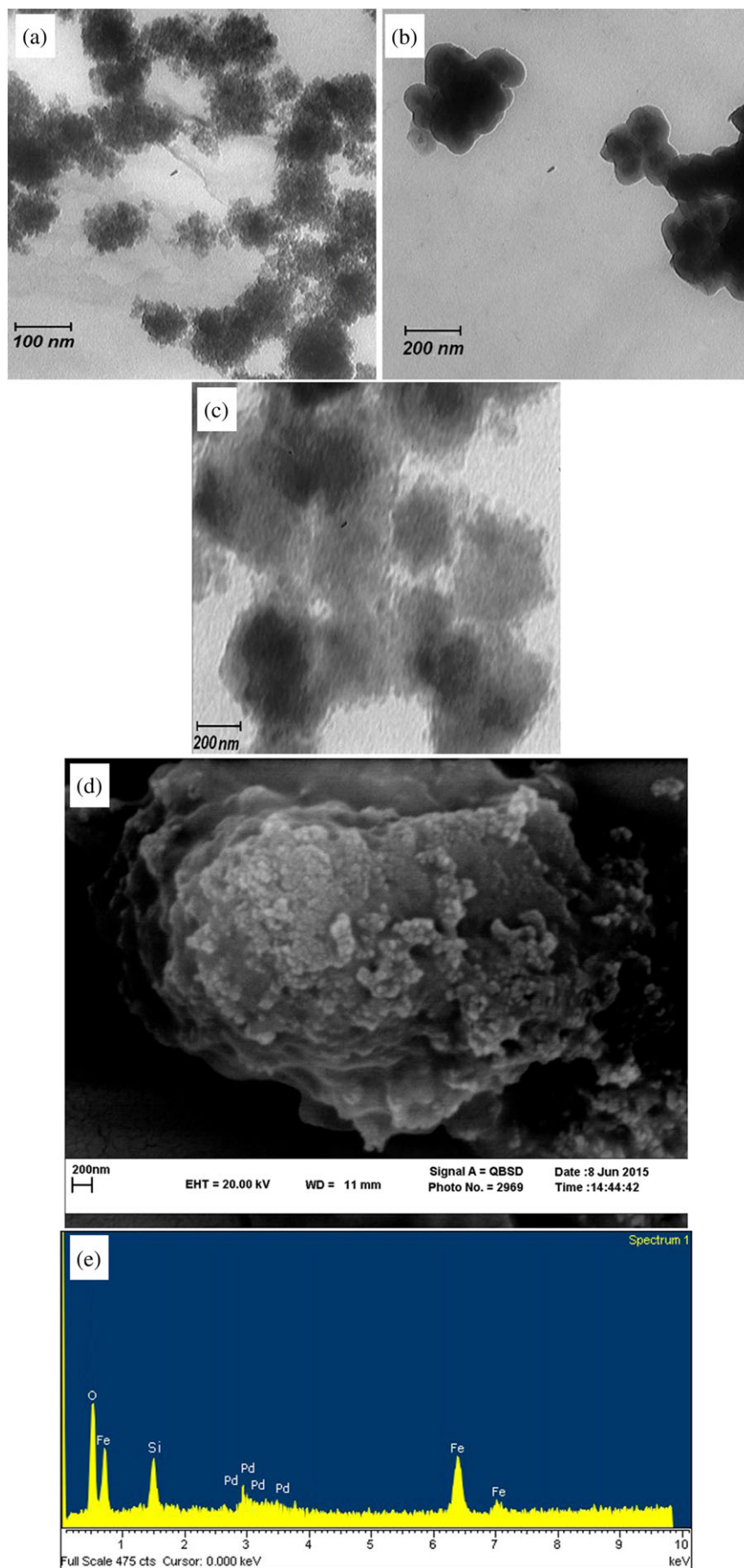
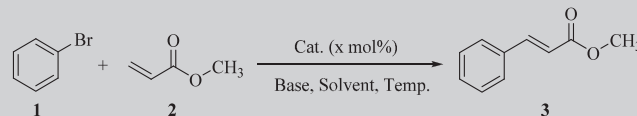


FIGURE 5 TEM images of (a) Fe₃O₄ MNPs, (b) FS MNPs and (c) FST-Pd⁰ MNPs. (d) SEM image of FST-Pd⁰ MNPs. (e) Energy-dispersive X-ray analysis of FST-Pd⁰ MNPs

TABLE 1 Optimization of model reaction catalysed by FST-Pd⁰ MNPs


| Entry | Catalyst (mol%) | Base | Solvent | Temp. (°C) | Time (h) | Yield of 3 (%) |
|-----------|-----------------|---------------------------------|-----------------------|------------|-------------|----------------|
| 1 | 1 | Na ₂ CO ₃ | DMF | 110 | 0.8 | 85 |
| 2 | 1 | Na ₂ CO ₃ | DMSO | 110 | 1.25 | 72 |
| 3 | 1 | Na ₂ CO ₃ | THF | 110 | 20 | 35 |
| 4 | 1 | Na ₂ CO ₃ | <i>n</i> -Hexane | 110 | 24 | 27 |
| 5 | 1 | Na ₂ CO ₃ | Toluene | 110 | 5 | 40 |
| 6 | 1 | Na ₂ CO ₃ | 1,4-Dioxane | 110 | 10 | 53 |
| 7 | 1 | Na ₂ CO ₃ | EtOH | 110 | 1 | 72 |
| 8 | 1 | Na ₂ CO ₃ | H ₂ O | 110 | 0.75 | 90 |
| 9 | 1 | — | H ₂ O | 110 | 24 | 0 |
| 10 | 1 | K ₃ PO ₄ | H ₂ O | 110 | 2 | 75 |
| 11 | 1 | KOH | H ₂ O | 110 | 1.25 | 60 |
| 12 | 1 | Et ₃ N | H ₂ O | 110 | 0.6 | 98 |
| 13 | 1 | Et ₃ N | H ₂ O | 80 | 0.66 | 97 |
| 14 | 0.5 | Et ₃ N | H ₂ O | 80 | 0.66 | 97 |
| 15 | 0.25 | Et₃N | H₂O | 80 | 0.66 | 96 |
| 16 | 0.1 | Et ₃ N | H ₂ O | 100 | 1.25 | 80 |
| 17 | 0.25 | Et ₃ N | H ₂ O | — | 24 | 5 |
| 18 | — | Et ₃ N | H ₂ O | 80 | 24 | — |
| 19 | FST (0.2 g) | Et ₃ N | H ₂ O | 80 | 24 | — |

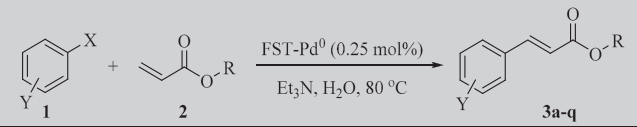
Reaction conditions: 1 mmol of bromobenzene, 1.2 mmol of methyl acrylate, 2 mmol of base, 1.5 ml of solvent.
bIsolated yield.

reaction time was achieved with 0.25 mol% of FST-Pd⁰ MNPs (Table 1, entry 15). Finally, the model reaction was conducted in the absence of any catalyst and also with FST MNPs. Results showed that under these conditions the reaction did not proceed (Table 1, entries 18 and 19). According to this study, water as solvent, Et₃N as base and 0.25 mol% of catalyst at 80°C were chosen as optimized reaction conditions.

The scope and adaptability of the catalysed Heck cross-coupling reaction were also investigated. The optimized reaction conditions were applied for the reaction of a wide range of aryl halides with electron-donating and electron-withdrawing groups with various olefins. The results (Table 2) revealed that cross-coupling reactions of various substituted aryl iodides and aryl bromides with methyl acrylate, ethyl acrylate and *n*-butyl acrylate proceeded to give high yields in short reaction time (Table 2, entries 1–17). Also, aryl halides with electron-withdrawing substituents react with olefins more quickly than those with electron-donating substituents. In the case of aryl chloride, a yield of only 40% of final cross-

coupled product was produced under the same reaction condition after 10 h (Table 2, entry 18).

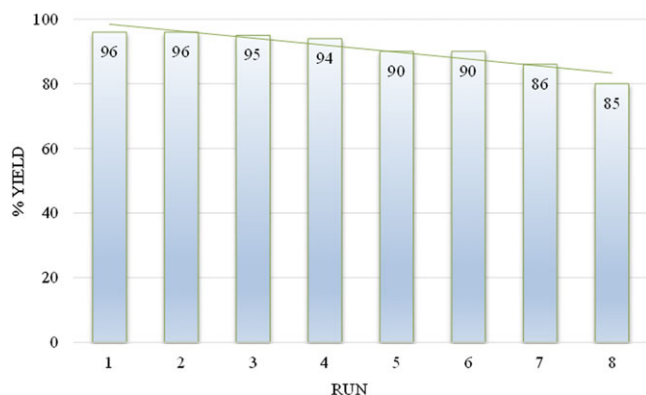
All of the products were known and isolated as oil or solid products which were characterized using NMR spectroscopy (see supporting information). The reaction progress was monitored by TLC and disappearance of starting substrates confirmed the completion of the reaction. For practical applications of heterogeneous catalysts and from a green chemistry point of view, the recovery and reusability of catalysts is an important factor. Furthermore, a set of experiments was conducted to recover and reutilize the FST-Pd⁰ MNPs in the model Heck cross-coupling reaction. After the first run, the FST-Pd⁰ nanocatalyst was easily separated from the reaction mixture using an external magnet and then washed with ethanol and ethyl acetate (3 × 5 ml). After drying the catalyst at 50°C in an oven, next model reaction was started using the recovered catalyst and fresh substrates. This process was repeated for eight consecutive runs (Figure 6). Results of hot filtration test for FST-Pd⁰ in the middle of the reactions show a low leaching of Pd after eight runs.

TABLE 2 Heck cross-coupling reaction of various substrates


| Entry | 1 | 2 | X | Time (min) | 3 | Yield (%) ^b |
|-------|---|---|------|------------|-----------|------------------------|
| 1 | | | I/Br | 25/40 | 3a | 96/96 |
| 2 | | | I/Br | 30/40 | 3b | 96/90 |
| 3 | | | I/Br | 35/45 | 3c | 96/94 |
| 4 | | | I/Br | 35/40 | 3d | 94/90 |
| 5 | | | I/Br | 30/45 | 3e | 92/92 |
| 6 | | | I/Br | 35/50 | 3f | 90/88 |
| 7 | | | I/Br | 35/45 | 3g | 93/90 |
| 8 | | | I/Br | 45/55 | 3h | 90/89 |
| 9 | | | I/Br | 25/30 | 3i | 94/92 |
| 10 | | | I/Br | 25/30 | 3j | 93/92 |
| 11 | | | Br | 35 | 3k | 91 |
| 12 | | | Br | 35 | 3l | 95 |
| 13 | | | I/Br | 40/35 | 3m | 91/90 |
| 14 | | | I/Br | 35/35 | 3n | 85/85 |
| 15 | | | I/Br | 25/25 | 3o | 94/90 |
| 16 | | | I | 25 | 3p | 95 |
| 17 | | | I/Br | 30/40 | 3q | 93/90 |
| 18 | | | Cl | 600 | 3a | 40 |

Conditions: **1** (1 mmol), **2** (1.2 mmol), base (2 mmol), catalyst (0.25 mol%), H₂O (1.5 ml), 80°C.

^bIsolated yield.

**FIGURE 6** Recyclability of catalyst for model reaction

The content of Pd on the recycled solid catalyst was measured using ICP-OES. Comparison between the amount of Pd in fresh and recycled catalyst revealed that only 0.05% of Pd species was leached after eight cycles.

4 | CONCLUSIONS


FST-Pd⁰ MNPs were synthesized and characterized as an environmentally friendly magnetic catalyst for Heck cross-coupling reaction of substrates with various electron-withdrawing and electron-donating groups on aromatic rings. Due to the high activity and efficiency of

this nanocatalyst, high yields in short reaction times were achieved. Probably, the presence of threonine with --NH₂ and --OH groups on the surface of the support led to well-dispersed Pd nanoparticles of small size. Uniformly dispersed small Pd nanoparticles resulted in high catalytic activity for the Heck reaction in water as a green, non-toxic solvent. The FST-Pd⁰ nanocatalyst after easy separation from the reaction mixture using an external magnet was reused for eight successful runs.

ACKNOWLEDGEMENTS

The authors gratefully acknowledged for partially financial support of this study by Ferdowsi University of Mashhad Research Council (Grant No: 3/41258).

ORCID

Mostafa Gholizadeh  <http://orcid.org/0000-0002-9947-2248>
 Mohammad Izadyar  <http://orcid.org/0000-0002-3795-9982>

REFERENCES

- [1] C. W. Lim, I. S. Lee, *Nano Today* **2010**, 5(5), 412.
- [2] Y. Nishina, K. Takami, *Green Chem.* **2012**, 14, 2380.
- [3] Z. L. Shen, H. L. Cheong, Y. C. Lai, W. Y. Loo, T. P. Loh, *Green Chem.* **2012**, 14(9), 2626.
- [4] K. Lamei, H. Eshghi, M. Bakavoli, S. A. Rounaghi, E. Esmaili, *Catal. Commun.* **2017**, 92, 40.
- [5] P. Bansal, G. R. Chaudhary, S. K. Mehta, *Chem. Eng. J.* **2015**, 280, 475.
- [6] J. Magano, J. R. Dunetz, *Chem. Rev.* **2011**, 111(3), 2177.
- [7] A. B. Dounay, L. E. Overman, *Chem. Rev.* **2003**, 103(8), 2945.
- [8] K. Lamei, H. Eshghi, M. Bakavoli, S. Rostamnia, *Appl. Organometal. Chem.* **2017**, 31(11).
- [9] T. E. Barder, S. D. Walker, J. R. Martinelli, S. L. Buchwald, *J. Am. Chem. Soc.* **2005**, 127(13), 4685.
- [10] K. Lamei, H. Eshghi, M. Bakavoli, S. Rostamnia, *Catal. Lett.* **2017**, 147(2), 491.
- [11] B. R. Vaddula, A. Saha, J. Leazer, R. S. Varma, *Green Chem.* **2012**, 14(8), 2133.
- [12] B. W. Glasspoole, J. D. Webb, C. M. Crudden, *J. Catal.* **2009**, 265(2), 148.
- [13] a) D. H. Lee, M. Choi, B. W. Yu, R. Ryoo, A. Taher, S. Hossain, M. J. Jin, *Adv. Synth. Catal.* **2009**, 351(17), 2912. b) S. Rostamnia, K. Lamei, F. Pourhassan, *RSC Adv.* **2014**, 4(103), 59626.
- [14] C. Burda, X. Chen, R. Narayanan, M. A. El-Sayed, *Chem. Rev.* **2005**, 105(4), 1025.
- [15] A. L. D. Ramos, P. da Silva Alves, D. A. Aranda, M. Schmal, *Appl. Catal., A* **2004**, 277(1–2), 71.
- [16] Q. Zhang, H. Su, J. Luo, Y. Wei, *Tetrahedron* **2013**, 69(2), 447.
- [17] C. M. Crudden, M. Sateesh, R. Lewis, *J. Am. Chem. Soc.* **2005**, 127(28), 10045.
- [18] D. H. Zhang, G. D. Li, J. X. Li, J. S. Chen, *Chem. Commun.* **2008**, (29), 3414.
- [19] V. G. Ramu, A. Bordoloi, T. C. Nagaiah, W. Schuhmann, M. Muhler, C. Cabrele, *Appl. Catal. A* **2012**, 431, 88.
- [20] O. V. Kharissova, B. I. Kharisov, V. M. Jiménez-Pérez, B. M. Flores, U. O. Méndez, *RSC Adv.* **2013**, 3(45), 22648.
- [21] A. Pal, I. Sevonkaev, B. Bartling, J. Rijssenbeek, D. V. Goia, *RSC Adv.* **2014**, 4(40), 20909.
- [22] F. Nador, M. A. Volpe, F. Alonso, A. Feldhoff, A. Kirschning, G. Radivoy, *Appl. Catal. A* **2013**, 455, 39.
- [23] a) I. Sarvi, M. Gholizadeh, M. Izadyar, *Catal. Lett.* **2017**, 147(5), 1162. b) W. Stöber, A. Fink, E. Bohn, *J. Colloid Interface Sci.* **1968**, 26(1), 62.
- [24] F. Taghavi, A. S. Saljooghi, M. Gholizadeh, M. Ramezani, *MedChemComm* **2016**, 7(12), 2290.
- [25] F. Taghavi, M. Gholizadeh, A. S. Saljooghi, *New J. Chem.* **2016**, 40(3), 2696.
- [26] F. Taghavi, M. Gholizadeh, A. S. Saljooghi, M. Ramezani, *MedChemComm* **2017**, 8(10), 1953.
- [27] D. Qi, H. Zhang, J. Tang, C. Deng, X. Zhang, *J. Phys. Chem. C* **2010**, 114(20), 9221.
- [28] A. S. Kashin, V. P. Ananikov, *J. Org. Chem.* **2013**, 78(22), 11117.

SUPPORTING INFORMATION

Additional supporting information may be found online in the Supporting Information section at the end of the article.

How to cite this article: Sarvi I, Gholizadeh M, Izadyar M. Threonine stabilizer-controlled well-dispersed small palladium nanoparticles on modified magnetic nanocatalyst for Heck cross-coupling process in water. *Appl Organometal Chem.* 2018;e4645. <https://doi.org/10.1002/aoc.4645>